HHS Public Access

Author manuscript

J Tissue Eng Regen Med. Author manuscript; available in PMC 2021 March 01.

Published in final edited form as:

J Tissue Eng Regen Med. 2020 March ; 14(3): 464–474. doi:10.1002/term.3007.

Mineralized Nanofibrous Scaffold Promotes Phenamil-induced Osteoblastic Differentiation while Mitigating Adipogenic Differentiation

Yangxi Liu[a], **Jue Hu**[b], **Hongli Sun**[b,*]

[a]Department of Biomedical Engineering, University of South Dakota, BioSNTR, Sioux Falls, SD 57107, USA

[b]Department of Oral and Maxillofacial Surgery, College of Dentistry, University of Iowa, Iowa City, IA 52242

Abstract

Large bone defects represent a significant unmet medical challenge. Cost-effectiveness and better stability make small molecule organic compounds a more promising alternative compared to bio-macromolecules, e.g., growth factors/hormones, in regenerative medicine. However, one common challenge for the application of these small compounds is their side-effect issue. Phenamil is emerging as an intriguing small molecule to promote bone repair by strongly activating BMP signaling pathway. In addition to osteogenesis, phenamil also induces significant adipogenesis based on some *in vitro* studies, which is a concern that impedes it from potential clinical applications. Besides the soluble chemical signals, cellular differentiation is heavily dependent on the microenvironments provided by the 3D scaffolds. Therefore, we developed a 3D nanofibrous bio-mimetic scaffold-based strategy to harness the phenamil-induced stem cell lineage differentiation. Based on the gene expression, ALP activity, and mineralization data, we indicated that bone-matrix mimicking mineralized-gelatin nanofibrous scaffold effectively improved phenamil-induced osteoblastic differentiation, while mitigated the adipogenic differentiation *in vitro*. In addition to normal culture conditions, we also indicated that mineralized-matrix can significantly improve phenamil-induced osteoblastic differentiation in simulated inflammatory condition. In viewing of the crucial role of mineralized matrix, we developed an innovative and facile mineral deposition-based strategy to sustain release of phenamil from 3D scaffolds for efficient local bone regeneration. Overall, our study demonstrated that biomaterials played a crucial role in modulating small molecule drug phenamil-induced osteoblastic differentiation by providing a bone-matrix mimicking mineralized gelatin nanofibrous scaffolds.

Graphical Abstract

[*]**Corresponding Author:** Professor Hongli Sun, Ph.D., Iowa Institute for Oral Health Research, Department of Oral and Maxillofacial Surgery, N405 DSB, College of Dentistry, 801 Newton Road, The University of Iowa, Iowa City, IA 52242, Tel: 319-335-1217, hongli-sun@uiowa.edu.

CONFLICT OF INTEREST

The authors have declared that there is no conflict of interest.

Phenamil is emerging as an intriguing small molecule to promote bone repair by strongly activating endogenous BMP signaling pathway for osteogenesis; however, phenamil also induces significant adipogenesis based on some *in vitro* studies, which is a concern that impedes it from potential clinical applications. Based on the comprehensive gene expression, ALP activity, and mineralization data, we indicated that bone-matrix mimicking mineralized-gelatin nanofibrous scaffold effectively improved phenamil-induced osteoblastic differentiation, while mitigated the adipogenic differentiation *in vitro*. In viewing of the crucial role of mineralized matrix, we developed an innovative and facile mineral deposition-based strategy to sustain release of phenamil from 3D scaffolds for efficient local bone regeneration.

Keywords

Adipogenesis; Hydroxyapatite; Osteogenesis; Phenamil; Scaffold

1. INTRODUCTION

Despite the natural healing of bone, critical-sized bone defects are unable to heal by itself thus represent an un-met medical challenge. Autograft, the gold standard of bone grafts, is commonly used as a surgical solution to solve large bone defects (Calori, Mazza, Colombo, & Ripamonti, 2011). Yet, bone grafts contain limitations such as donor-site morbidity and postoperative pain and infection (Guerado & Caso, 2017). Bone tissue engineering aims to provide alternative treatments for critical-sized defects through the combination usage of cells, scaffolds, and signaling molecules (Laurencin, Ashe, Henry, Kan, & Lo, 2014).

Signaling molecules such as small molecule compounds are becoming a more promising alternative compared to bio-macromolecules in regenerative medicine (W.H. Lo, D. Ulery, Deng, M. Ashe, & T. Laurencin, 2011). Bone morphogenetic proteins (BMPs) were traditional macromolecules adopted in drug delivery for bone repair, where BMP2 and

BMP7 became FDA-approved osteoinductive growth factors for clinical use (Hankenson, Gagne, & Shaughnessy, 2015). Bio-macromolecules present inadequacies in its usage such as high cost, immunogenicity, and structural instability (Lo, Ashe, Kan, & Laurencin, 2012), therefore, additional therapeutic approach are being explored for bone regeneration. Cost-effective, less immune response, and better stability, small molecules (i.e. phenamil, icariin, psoralen) have made strides in recent times as effective therapy when utilized as drug delivery for bone tissue engineering by inducing osteogenic differentiation markers (Awale, Wong, Rajpura, & K, 2017). Delivery systems for small molecules has been tailed by application utilizing various methods such as sponge, beads, nano- and micro-particles or 3D scaffold (Balmayor, 2015). However, small molecules may present certain challenges including nonspecific cell targeting and adverse side-effects (Lo et al., 2012). Phenamil, an osteo-inducer, is emerging as an intriguing small molecule for bone repair through strong BMP-signaling pathway activation (Fan et al., 2015; Miszuk et al., 2018) to direct intracellular signaling by provoking tribbles homolog 3 (Trb3) activation. Trb3 can downregulate Smad-Specific E3 Ubiquitin Ligase 1 (SMURF1), a BMP antagonist, and thus stabilize Smad, a BMP signaling inducer (Chan et al., 2007), to promote phenamil as a promising small molecule for bone formation (Fan et al., 2015). However, phenamil also induces adipogenesis via stimulation of peroxisome proliferator-activated receptor γ (PPARγ), a master transcriptional regulator of adipogenesis (Park, Waki, Choi, Park, & Tontonoz, 2010; Tontonoz, Hu, & Spiegelman, 1994). Phenamil-induced adipogenesis is a severe concern that impedes it from potential clinical applications. Therefore, we should develop innovative strategy to address the challenges of phenamil-induced stem cell differentiation.

Aside from soluble chemical signals, cellular differentiation is heavily dependent on the physical cues within the microenvironment. Physical stimulus (e.g. matrix shape and stiffness) can modulate stem cell behavior including cell attachment resulting in flatten and spread-shaped and cell differentiation such that rigid matrix topography directed mesenchymal stem cells (MSCs) to differentiate osteogenically even if cells are provided similar chemical differentiation medium (Engler, Sen, Sweeney, & Discher, 2006; McBeath, Pirone, Nelson, Bhadriraju, & Chen, 2004). It has been well-known that hydroxyapatite (HA), major inorganic part of bone tissue, with similar chemical components to bone mineral showed strong improvement of BMP2-induced osteoblast differentiation by upregulating alkaline phosphatase and BSP expression possibly through improved stiffness (Miszuk et al., 2018; Yang, Li, Liu, Zhang, & Feng, 2018). Biomineralized matrices dominate soluble cues to promote osteogenic differentiation under adipogenic-inducing media by regulating mesenchymal stem cell osteoblastic differentiation (Shih et al., 2014; Wen et al., 2012). Physical catalysts from synthetic mineral-based matrices modulate stem cell differentiation towards specific phenotype while inhibiting differentiation into other lineages (Kang, Shih, & Varghese, 2015). Therefore, mineral-mimicking scaffold plays a key role in bone tissue engineering, may present a physiological way to modulate drug-induced stem cell lineage both physically (e.g. topography, stiffness) and chemically (minerals).

In present work, our hypothesis is 3D nanofibrous bone matrix-mimicking mineralized gelatin (HAGF) scaffold is a promising solution for phenamil-induced osteogenesis for bone

tissue engineering. Bone-matrix mimicking mineralized gelatin scaffold enhanced alkaline phosphatase (ALP) activity and mineralization for osteogenesis, whilst downregulating phenamil-induced adipogenic gene expression in vitro. Our study demonstrated the active roles of biomaterials in modulating phenamil-induced lineage differentiation by mineralized-matrix gelatin scaffold.

2. MATERIAL AND METHODS

2.1. Materials

Acetone, methylene chloride, ethanol, 1, 4-dioxane, Triton-X 100, formaldehyde, and hexanes, glycine were purchased from Fisher Scientific (NJ, USA). Gelatin type B (from bovine skin, 225 Bloom), (2-(N-morpholino)ethanesulfonic acid) hydrate (MES), N-hydroxysuccinimide (NHS), alkaline phosphatase kit, lipopolysaccharide (LPS) from Escherichia coli, sodium citrate, ascorbic acid, β-glycerol-2-phosphate, polyvinylalcohol and cyclohexane were purchased from Sigma (St. Louis MO, USA). 1-Ethyl-3-(3-dimethylaminopropyl) carbodiimide HCl (EDC), bicinchoninic acid assay kit (BCA), and GeneJET RNA purification were purchased from Thermal Scientific (Rockford, USA). Phenamil (methanesulfonate) were purchased from Cayman Chemical (Cayman Chemical, MI, USA). MC3T3-E1 cells and C3H/10T1/2 cells were cultured in alpha-MEM (Gibco, Maryland, USA). Osteo-conductive (OC) media was prepared using alpha-MEM base media with the addition of β-glycerol-2-phosphate (10 mM) and ascorbic acid (50μM). Adipogenic media was prepared using DMEM as base media with fetal bovine serum and penicillin-streptomycin and troglitazone (5μg/mL), insulin (167nM), 3-isobutyl-1-methylxanthine (50μM), and dexamethasone (1nM).

2.2. Preparation of Gelatin Scaffold

3D gelatin nanofibrous (GF) scaffolds were prepared using paraffin spheres according to previous reports (Y. Liu, Yao, & Sun, 2018; Q. Yao, Liu, & Sun, 2018; Q. Yao, Liu, Tao, Baumgarten, & Sun, 2016) with some modifications. Briefly, 1.0 g paraffin spheres with a diameter size between 300–500 μm were added to Teflon molds (φ17 mm cylinder) and preheated at 37 °C for 28 minutes. A 10 wt.% gelatin solution, using 50% ethanol/water as solvent, was cast onto the interconnected paraffin spheres. After four hours of phase separation at −80 °C, samples were immersed overnight in ethanol at −20 °C and then soaked in 1, 4-dioxane solution at room temperature overnight with rotation and subsequently frozen again and then lyophilized in salt-ice bath. Gelatin-paraffin scaffolds were cut into ϕ 5 mm ×1 mm discs and then washed with hexanes and then cyclohexane at room temperature with agitation. Samples were frozen again at −20 °C overnight and lyophilized and stored until further use in desiccator.

Chemical crosslinking of 3D GF and HAGF scaffolds were carried out in the MES buffer (pH 5.3, 0.05 M) with EDC and NHS as crosslinking solution. To preserve nanofiber nanostructure and prevent swelling, scaffolds were soaked in 40mL of cold acetone in vial. Crosslinking solution (2mL) was added to scaffolds soaked acetone and shaken on ice overnight. Then another 2mL of crosslinking solution was added next day and shaken on ice overnight again. After crosslinking, the gelatin scaffolds were washed with glycine and then

distilled (DI) water 3 times, then frozen at −20 °C overnight and lyophilized and stored in a desiccator.

For cell culture, sterilization of 3D GF or HAGF scaffold was done by ethanol sterilization. Briefly, scaffolds were soaked in 70% ethanol solution for one hour. Then the scaffold was washed for thirty minutes in DPBS one time and then washed once with molecular-free water for 30 minutes. Then scaffold was soaked in medium and placed in incubator at 37°C, 5% CO_2 until use.

2.3. Mineralization of GF scaffold

Gelatin nanofibrous scaffolds were first crosslinked and then coated with calcium phosphate through either a one-step or two-step deposition process. Mineral deposition was prepared according to previous protocols with some modifications (Kang et al., 2015; X. Liu & Ma, 2009; Oyane et al., 2003).

In one-step deposition, scaffolds were deposited with hydroxyapatite via a concentrated (10X) simulated body fluid (SBF). Scaffolds were wetted beforehand in sodium citrate (0.1M) solution for an hour. Then scaffolds were transferred into a glass vial with simulated body fluid and is shaken at 37°C for four hours. Afterwards, the scaffold is dehydrated with 1,4-dioxane with rotation for an hour. The scaffolds were then frozen in −80°C and lyophilized overnight. Concentrated simulated body fluid (10X) is prepared by adding ingredients to 475 mL of DI water at room temperature, allowing each ingredient to fully and completely dissolve before adding the next. The components are NaCl (29.22g), KCl (0.19g), $CaCl_2$ (anhydrous) (1.38g), $MgCl_2 \cdot 6H_2O$ (0.58g), $NaH_2PO_4 \cdot 2H_2O$ (0.28g), and $NaHCO_3$ (0.42g). After the final ingredient completely dissolves, adjust volume to 500 mL by adding DI water using graduated cylinder. Return solution to beaker and adjust pH to 6.0 using HCl and NaOH as necessary. Store solution in plastic bottle with tightly sealed cap in refrigerator up to one week. One-step (10X SBF) hydroxyapatite-deposited scaffold was used for all experiments except for drug release (Figure 6).

Two-step calcium phosphate deposition process is done through a combination of nucleation solution and propagation solution. GF scaffold is pre-treated for one hour in sodium citrate solution and then soaked in nucleation solution for three hours under rotation at 37°C. Afterwards, the GF scaffold was washed with DI water and frozen then freeze-dried overnight. Nucleation solution (step 1) is comprised of NaCl (19.95g), $CaCl_2$ (anhydrous, 0.69g), $NaH_2PO_4 \cdot 2H_2O$ (0.45g), $NaHCO_3$ (0.88g), $MgCl_2 \cdot 6H_2O$ (0.76g). After the final ingredient completely dissolves, adjust the final volume to 500 mL by adding DI water. No pH adjustment is necessary. After, dried scaffolds were then immersed in propagation solution the next day and shaken at 37°C for another 24 h. Scaffolds were washed again and frozen and lyophilized overnight. Propagation solution (step 2) is comprised of 2.5mL HCl (10M), $CaCl_2$ (anhydrous, 0.22g), NaCl (3.98g), $NaH_2PO_4 \cdot 2H_2O$ (0.18g) in 500mL of DI water. After all is dissolved, solution is adjusted to pH of 7.4 using Tris Base and stored up to 2 weeks at 4°C. After propagation solution immersion, HAGF scaffold was frozen and lyophilized overnight and kept in desiccator until use.

2.4. Characterization of GF scaffold

The morphology and microstructure of 3D scaffolds were characterized through Quanta Standard Environmental SEM (FEI, United States). Mechanical compression used MTS insight (MTS, MN, USA) machine according to previous reports (X. Liu & Ma, 2009; Xu, Miszuk, Zhao, Sun, & Fong, 2015; Q. Yao et al., 2016) with some modifications. Briefly, a sample was placed under the loading cell with 60% of weight (up to 1 kN) applied. All samples were circular discs (5mm in diameter and 1.5mm in thickness). The averages and standard deviations were reported.

Fourier-transform infrared spectroscopy (Thermo Scientific, MA, USA) determined the absorption on an infrared spectrum. Confocal microscopy imagining of MC3T3-E1 in both scaffold at a cell density of 75×10^3 cells per scaffold were performed according to previous reports (Y. Liu et al., 2018). Cell-seeded scaffold was cultured for five days in growth medium. Cells were fixed and stained with Texas Red-X Phalloidin (Molecular Probes, NY) and DAPI (SouthernBiotech, AL) according to the manufacturer's manual. Stained cells were observed under confocal microscopy (FV1200, Olympus, Japan).

2.5. Assay analysis

Alkaline phosphatase enzymatic activity was quantified and qualified following previous method (Y. Liu et al., 2018; Miszuk et al., 2018; Q. Yao, Liu, Selvaratnam, Koodali, & Sun, 2018; Q. Yao, Liu, & Sun, 2018; Q. Yao et al., 2016). ALP staining images were taken via camera. ALP quantitative measurements used sensolyte pNPP alkaline phosphatase assay kit. Microplate reader was used to record the absorbance at 405nm.

MC3T3-E1 and C3H/10T1/2 was (purchased from ATCC) used to study osteogenesis and adipogenesis. Calcium deposition measurement use total calcium LiquiColor® kit (Stanbio laboratory, TX) as we described previously (Y. Liu et al., 2018). Briefly, cells/scaffolds were rinsed with DPBS and immersed in 1N hydrochloric acid and tested according to the manufacturer's instruction. The absorbance was measured at 550 nm, and the calcium content was calculated. Oil red O measured at 500 nm with 0.5 s per reading using microplate reader. Briefly, media was removed and 10% formalin was added to each well and incubated at room temperature for at least an hour. Next, remove all formalin and wash with 60% isopropanol and then let wells dry completely. Then add in oil red O working solution to each well and incubate for 10 min with rotation. Wells were then washed with DI water. Oil red O can be eluted using pure isopropanol after 10 min incubation and analyzed.

2.6. Phenamil Release

In vitro drug release was prepared as previous methods with modifications. HAGF-Phe-Abs (absorbed phenamil) and HAGF-Phe-Enc (encapsulated phenamil) scaffolds were studied for *in vitro* phenamil release. For HAGF-Phe-Abs scaffold, 10 μL of 20 μM phenamil solution was added to HA scaffold and freeze dried. HAGF-Phe-Enc scaffolds were prepared by immersing nucleated scaffolds into propagation solution (2 mL) with phenamil for overnight HAGF-Phe deposition and then freeze-dried. Lyophilized scaffolds were then immersed in 1 mL PBS solution at 37 °C on an orbital shaker at 100 rpm. After 28 days of release, the amount of Phenamil released was determined by microplate reading at 366 nm.

Encapsulation efficiency for HAGF-Phe-Enc scaffold was calculated from formula: encapsulation efficiency (%) = [(total drug added − free non-trapped drug) / total drug added] * 100.

2.7. Gene expression analysis

Quantitative gene expression analysis was carried out as we previously described (Y. Liu et al., 2018; Q. Yao, Liu, & Sun, 2018; Q. Yao et al., 2016) with some minor modifications. Briefly, total RNA was extracted using the GeneJET™ RNA Purification Kit (Thermo Scientific™, Waltham, MA). RNA concentration was measured by UV–Vis spectroscopy (DU 730, Beckman coulter) at 260 nm and 280 nm and an equivalent amount of RNA was processed to generate cDNA by using the High Capacity cDNA Reverse Transcript kit purchased from Applied Biosystems (Forster City, CA). Quantitative PCR was performed with Taqman gene expression assays (Applied Biosystems, Forster City, CA) using the Applied Biosystems 7500 Fast Real-Time PCR System (Applied Biosystems, Carlsbad, CA). Triplicates were performed for each sample, and results were normalized to GAPDH. TaqMan® Gene Expression Assays of GAPDH (Mm99999915), RUNX2 (MmCG122221) and OCN (Mm03413826), PPARγ (Mm00440940), Fabp4 (Mm00445878), LPL (Mm00434764) were purchased from Applied Biosystems (Forster City, CA).

2.8. Statistical Analysis and Image Editing

Statistical significance of observed differences between the study groups used a two-tailed homoscedastic *t-test* was applied. A value of $p < 0.05$ was statistically significant while $0.05 < p < 0.10$ was considered to represent a non-significant, but clear trend in cell or tissue response. Values are reported as the mean ± standard deviation (SD). Brightness and contrast were adjusted equally across all images for improved visibility.

3. RESULTS

Bio-mineralization of gelatin nanofibrous scaffold

Gelatin nanofibrous scaffold was constructed according to previous protocols with nanofibrous physique on struts and pore surfaces (X. Liu & Ma, 2009; Q. Yao et al., 2016; Qingqing Yao, Sandhurst, Liu, & Sun, 2017). GF scaffold fabricated well-interconnected pores and a well-defined macro-porous physical structure (Figure 1A). Nanofibrous formation on gelatin scaffold is formed through the phase separation of two different liquid solvents during thermally induced phase separation (TIPS) thus generating nanfibrous, which is can be seen at high magnification (Figure S5). Previous, we depicted nanofiber characteristics through fiber diameter and length (Q. Yao et al., 2016). Highly porous 3D GF scaffolds were then treated with concentrated simulated body fluid for calcium phosphate deposition to emulate hydroxyapatite (Figure 1B–C). SEM images displayed hydroxyapatite-flake like morphology at high magnification. Hydroxyapatite surface coating was confirmed through FTIR spectroscopy analysis detected both gelatin and HA identifiable peaks on HAGF scaffold (Figure 1D). Gelatin characteristic peaks were found with C-H stretching from amide B at 2923 cm^{-1}, N-H stretching of amide A band at 3299 cm^{-1}, and a N-H deformation of the amide II at 1536 cm^{-1} (Qadir, Jakir Hossan, Gafur, & Mainul Karim, 2014). An evident carbonyl stretching (C=O) at 1627 cm^{-1} is observed and a

usual peak at 1333 cm^{-1} indicating the wagging vibration of proline side chains. Typical hydroxyapatite FTIR peaks showed carbonate V2 band at 878 cm^{-1} and various CO_3 V3 bands in 1580–1350 cm^{-1} range. Distinct phosphate bands exhibited with 963 cm^{-1} phosphate υ1 band, 469 cm^{-1} phosphate υ2 band, 600 and 559 cm^{-1} phosphate υ4 bands and 1090 and 1020 cm^{-1} phosphate υ3 bands (S M Arsad, M Lee, & Kong Hung, 2011) (Figure S3). Mechanical compression testing utilized cylindrical scaffold disks (2.5 mm r × 1 mm h) and showed HAGF scaffold, albeit statistically insignificant, trended towards a higher mechanical strength than GF scaffold (Figure 1E).

HAGF scaffold similarly promoted material to cellular interaction as GF scaffold, where cell attachment is favorable in HAGF scaffold with no noticeable cell morphology variation of MC3T3-E1 cells observed in both GF and HAGF scaffold under SEM after 24 h cell culture (Figure S1). Consistently, MC3T3-E1 cells penetrated scaffold as confocal scaffold cross-section showed (Figure 2 E–F). Confocal imaging via z-stack displayed more cell attachment and penetration in GF and HAGF scaffold to sustain MC3T3-E1, stained for visualization, after 5 d (Figure 2 A–D).

Hydroxyapatite Scaffold Modulation of Phenamil-Induced Adipogenesis

Phenamil-induced adipogenic differentiation were examined on C3H/10T1/2 for cell activity with and without treatment. C3H10T1/2 cells during adipogenic studies were cultured in adipogenic medium. C3H10T1/2 cells were treated with various concentrations of phenamil in adipogenic medium against a growth medium control group to confirm increased lipid content with phenamil concentration of 0 μM (Figure 3A) and 20 μM (Figure 3B) after oil red O staining (Figure 3 A–B). Quantitative results showed significant increase in lipid content as phenamil concentration increased (Figure 3C). Both oil red staining and quantification are performed on 2D culture plates.

Furthermore, adipogenic gene expression were evaluated on GF and HAGF scaffolds either with or without the presence of phenamil in adipogeneic medium. Consistent with the 2D culture, our data indicated that phenamil can increase all the adipogenic markers on both GF and HAGF scaffolds. Importantly, our data showed HAGF scaffold alone significantly decreased gene markers: peroxisome proliferator-activated receptor gamma (PPARγ), fatty acid-binding protein (Fabp4) and lipoprotein lipase (LPL). HAGF scaffolds with phenamil (HAGF-Phe) at 20 μM concentration also downregulated phenamil-elevated adipogenic gene expression on 3D matrices (Figure 3D–F).

MC3T3-E1 Osteoblastic Differentiation on HAGF Scaffold

Phenamil demonstrated a significant concentration-dependent increase of alkaline phosphatase activity in the pre-osteoblasts, MC3T3-E1 cells both qualitatively (staining, Top Left Panel) and quantitatively (Top Right Panel, Figure 4).

Osteogenic gene expressions of MC3T3-E1 were analyzed in GF and HAGF scaffold with and without phenamil treatment. Surprisingly, HAGF scaffold significantly decreased runt-related transcription factor 2 (RUNX2) expression without and with phenamil at 20 μM (Figure 4C) on day 7. Conversely, HAGF scaffold significantly increased osteocalcin (OCN) and bone sialoprotein (BSP) expression and HAGF-Phe scaffold significantly increased BSP

expression only (Figure 4D–E). At 14 d, HAGF scaffold significantly upregulated OCN and BSP expression with and without phenamil addition (Figure 4G–H). However, RUNX2 gene expression at 14 d provided paradoxical results, where HAGF scaffold significantly increased expression while HAGF-Phe significantly decreased its gene expression (Figure 4F).

To further study the effects of phenamil and hydroxyapatite on osteoblastic differentiation in an inflamed condition, we used LPS to mimic the inflammatory microenvironment. As our data indicated, LPS significantly inhibited the ALP activity of MC3T3-E1 at both high (2 μg/mL, L2) and low (10 ng/mL, L10) concentration. Phenamil could significantly improve ALP activity and largely rescue LPS-inhibited osteoblastic differentiation (Figure 5A).

Consistently, LPS also significantly inhibited calcium mineral formation. Alizarin red S analysis exhibited both phenamil and BMP2 were capable of significantly rescuing LPS-inhibited calcium mineralization (Figure 5B). Results indicated phenamil recovered LPS-restricted osteogenic differentiation in early ALP activity and calcium mineralization. 3D cell culture of MC3T3-E1 on GF and HAGF scaffold was analyzed for total calcium content. HAGF scaffold indicated significantly increased cell mineralization in all groups compared to GF-based scaffold cell culture, while HAGF-Phe scaffold rescued LPS-inhibited calcium mineralization (Figure 5C). Blank scaffolds of both GF and HAGF were immersed in media for 28 d and no significant scaffold calcium content was observed (Figure S4).

Phenamil Release from Scaffold

Phenamil, a hydrophobic compound, was released from HAGF scaffold by physical absorption or encapsulation within HA crystal. Phenamil encapsulation utilized two-step calcium phosphate deposition that provided similar chemical composition via FTIR analysis (Figure S2) and HA flake-like morphology under SEM (Figure 6B). Phenamil incorporation did not alter scaffold morphology and both physical absorption and encapsulation phenamil groups utilized two-step HA coating scaffolds. Encapsulation efficiency was calculated at an average of 57.4% (~11.5ug) for HAGF-Phe-Enc scaffold from using the encapsulation solution to test for free non-entrapped drug via microplate reading. Physically absorbed phenamil on HAGF scaffold showed initial burst release within the first eight hours of release with up to 74% of phenamil released. While HAGF scaffold with phenamil encapsulated within hydroxyapatite deposition provided similar release amount (73%) over 21 d periods (Figure 6C).

4. DISCUSSION

Phenamil is a small molecule that assist bone repair through osteogenic differentiation; however, phenamil induced-adipogenic differentiation, could be a significant issue for bone repair, has been less extensively investigated. Herein, we demonstrated the novel contribution of hydroxyapatite on phenamil-induced stem cell lineage differentiation to improve osteogenesis and reduce fat accumulation during bone formation by using a 3D bone mineral-matrix mimicking nanofibrous gelatin scaffold. In viewing of the crucial role of mineralized matrix, we developed an innovative and facile mineral deposition-based

strategy to sustain release of phenamil from 3D scaffolds for efficient local bone regeneration.

To fully investigate phenamil adipogenic and osteogenic differentiation, lipid content, alkaline phosphatase, gene expression and calcium mineralization were examined in both C3H10T1/2 and MC3T3-E1 cells. Multipotent C3H10T1/2 cells were initially used to represent mesenchymal stem cells for both adipogenic and osteogenic differentiation but C3H10T1/2 cells fail to produce mineralization as previous studies dictated (Katagiri et al., 1990). Thus MC3T3-E1 was used to examine late stages of osteoblastic differentiation, where it is well suited due to mineralized bone nodule formations (Yamaguchi, Sakamoto, Minamizato, Katsube, & Nakanishi, 2008). Additionally, the use of multiple cellular phenotypes provides more relatable information on cellular lineage differentiation study during bone healing and regeneration and demonstrates phenamil-induced lineage differentiation across multiple cell types. Both cell types respond to phenamil in a concentration dependent manner.

Our research showed the ability to use HA-modified materials for not only improvement of phenamil-induced osteogenesis, but also inhibition of the adipogenesis, which has been minimally studied previously. HA increased ALP activity yet osteogenic RUNX2 marker did not upregulate with phenamil treatment at both time points. A possible explanation may be that past report dictated ALP could be stimulated in RUNX2-definicent cells suggesting an independent mechanism of action for ALP and RUNX2 (Komori et al., 1997). In 3D, HAGF scaffold upregulated osteogenic differentiation due to the biomineral-matrix containing calcium phosphate that increased osteogenic activity by possible targeting adenosine A2b receptor (A2bR) to specify osteogenic differentiation (Carroll et al., 2012; Shih et al., 2014).

Excessive or chronic inflammation is known to be detrimental for tissue regeneration, including bone repair by causing bone loss (Loi et al., 2016). It is crucial to examine phenamil osteogenic ability under inflamed condition to investigate full efficacy of small molecule in comparison to conventional bio-macromolecules in bone regeneration. LPS, gram-negative bacteria endotoxin, is used to simulate chronic inflammation *in vitro* and inhibits osteoblastic differentiation in MC3T3-E1 cells through c-Jun N-terminal kinases (JNK) pathway reproducing possible inflammation related damage in dental or bone healing (Guo et al., 2014). Under simulated inflammatory microenvironment, phenamil rescued LPS-inhibited ALP activity and calcium content. HAGF-Phe scaffold rescued LPS-inhibited mineralization as well. The rescuing ability of phenamil is in accordance with previous reports showing phenamil has anti-inflammatory properties because phenamil activates Trb3, a negative regulator of pro-inflammatory cytokines (Fan et al., 2015). Pro-inflammatory cytokines such as IL-1, TNFα, and IL-6 are expressed by activation of nuclear factor kappa-light-chain-enhancer of activated B cells or NF-κB, which can be significantly suppressed by phenamil (Chang et al., 2013). The ability of phenamil to upregulate Trb3 to increase osteogenesis and decrease inflammatory reaction by signaling pathway inhibition confirmed our results showing rescuing of LPS-inhibited osteogenic activity.

Sustained drug delivery depicts the release of a drug from a delivery vehicle at a calculated rate to preserve efficacy. Phenamil, a lipid compound, poses a challenge in drug delivery

when incorporating onto a 3D scaffold matrix. Biomimetic mineral deposition on scaffolds is ideal for drug delivery by encapsulation of bioactive agents into the HA crystalline lattice network while having intrinsic osteo-inductive properties (Y. Liu, Hunziker, Randall, de Groot, & Layrolle, 2003). Our HA-deposited scaffold entrapped phenamil molecules diminished the burst-release effect, while maintaining cumulative release percentage over time. HA encapsulation of phenamil onto GF scaffold for drug release is optimal in that the deposition process is performed in very mild conditions so to not deform the scaffold; simultaneously, HA crystals perform sustained and localized phenamil-release that will require lower phenamil dosage and reduced cytotoxicity and maintaining long-period phenamil release is conducive since bone regeneration requires longer healing time. Entrapment of hydrophobic drug within mineral crystals aim to provide a unique method to uphold drug concentration within the therapeutic window.

Based on our current work, we believe mineral-based sustained release is important for phenamil's application to bone tissue engineering. Mineralized scaffold not only reduce burst-release related toxicity but also improve osteoblastic differentiation through reducing adipogenic differentiation. It is well known that osteoblast and adipocyte share the same progenitors-MSCs. Biomimetic HAGF scaffold employ HA mineral to maintain phenamil bioactivity and work synergistically with phenamil to promote osteogenesis, while inhibiting adipogenesis.

5. CONCLUSION

Overall, we employed a 3D bone-matrix mineralized gelatin nanofibrous scaffold for phenamil-induced osteogenesis for bone tissue engineering. HA mineral successfully deposited onto GF scaffold via either concentrated SBF (one-step) or two-step mineral deposition process. Our data indicated HAGF scaffold significantly inhibited phenamil-induced adipogenic gene expression. Furthermore, mineralized scaffold/phenamil can significantly improve osteoblastic differentiation in both normal and inflammatory conditions. Mineral-encapsulated phenamil showed a simple and moderate sustained release curve mitigating initial burst release. Our study, for the first time, demonstrated bone-matrix mineralized gelatin scaffold regulate phenamil-induced stem cell lineage differentiation.

Supplementary Material

Refer to Web version on PubMed Central for supplementary material.

ACKNOWLDEGMENTS

Financial support for this work was from the National Institutes of Health /NIDCR (Award Number: R03 DE027491 to HS), and the National Science Foundation/EPSCoR (Award IIA1335423).

Reference:

Abhishek D, Ghule P, & Aher A (2017). SUSTAINED RELEASE DOSAGE FORM: A CONCISE REVIEW (Vol. 5).

Awale G, Wong E, Rajpura K, & W. H. L. K (2017). Engineered Bone Tissue with Naturally-Derived Small Molecules. Curr Pharm Des, 23(24), 3585–3594. doi:10.2174/1381612823666170516145800 [PubMed: 28521690]

Balmayor ER (2015). Targeted delivery as key for the success of small osteoinductive molecules. Adv Drug Deliv Rev, 94, 13–27. doi:10.1016/j.addr.2015.04.022 [PubMed: 25959428]

Calori GM, Mazza E, Colombo M, & Ripamonti C (2011). The use of bone-graft substitutes in large bone defects: Any specific needs? Injury, 42, S56–S63. doi:10.1016/j.injury.2011.06.011 [PubMed: 21752369]

Carroll SH, Wigner NA, Kulkarni N, Johnston-Cox H, Gerstenfeld LC, & Ravid K (2012). A2B adenosine receptor promotes mesenchymal stem cell differentiation to osteoblasts and bone formation in vivo. J Biol Chem, 287(19), 15718–15727. doi:10.1074/jbc.M112.344994 [PubMed: 22403399]

Chan MC, Nguyen PH, Davis BN, Ohoka N, Hayashi H, Du K, … Hata A (2007). A novel regulatory mechanism of the bone morphogenetic protein (BMP) signaling pathway involving the carboxyl-terminal tail domain of BMP type II receptor. Mol Cell Biol, 27(16), 5776–5789. doi:10.1128/mcb.00218-07 [PubMed: 17576816]

Chang J, Liu F, Lee M, Wu B, Ting K, Zara JN, … Wang CY (2013). NF-kappaB inhibits osteogenic differentiation of mesenchymal stem cells by promoting betacatenin degradation. Proc Natl Acad Sci U S A, 110(23), 9469–9474. doi:10.1073/pnas.1300532110 [PubMed: 23690607]

Engler AJ, Sen S, Sweeney HL, & Discher DE (2006). Matrix elasticity directs stem cell lineage specification. Cell, 126(4), 677–689. doi:10.1016/j.cell.2006.06.044 [PubMed: 16923388]

Fan J, Im CS, Cui ZK, Guo M, Bezouglaia O, Fartash A, … Lee M (2015). Delivery of Phenamil Enhances BMP-2-Induced Osteogenic Differentiation of Adipose-Derived Stem Cells and Bone Formation in Calvarial Defects. Tissue Eng Part A, 21(13–14), 2053–2065. doi:10.1089/ten.TEA.2014.0489 [PubMed: 25869476]

Gharibi B, Abraham AA, Ham J, & Evans BA (2011). Adenosine receptor subtype expression and activation influence the differentiation of mesenchymal stem cells to osteoblasts and adipocytes. J Bone Miner Res, 26(9), 2112–2124. doi:10.1002/jbmr.424 [PubMed: 21590734]

Gharibi B, Abraham AA, Ham J, & Evans BA (2012). Contrasting effects of A1 and A2b adenosine receptors on adipogenesis. Int J Obes (Lond), 36(3), 397–406. doi:10.1038/ijo.2011.129 [PubMed: 21730968]

Guerado E, & Caso E (2017). Challenges of bone tissue engineering in orthopaedic patients. World J Orthop, 8(2), 87–98. doi:10.5312/wjo.v8.i2.87 [PubMed: 28251059]

Guo C, Yuan L, Wang JG, Wang F, Yang XK, Zhang FH, … Song GH (2014). Lipopolysaccharide (LPS) induces the apoptosis and inhibits osteoblast differentiation through JNK pathway in MC3T3-E1 cells. Inflammation, 37(2), 621–631. doi:10.1007/s10753-013-9778-9 [PubMed: 24272171]

Hankenson KD, Gagne K, & Shaughnessy M (2015). Extracellular signaling molecules to promote fracture healing and bone regeneration. Adv Drug Deliv Rev, 94, 3–12. doi:10.1016/j.addr.2015.09.008 [PubMed: 26428617]

Kang H, Shih YR, & Varghese S (2015). Biomineralized matrices dominate soluble cues to direct osteogenic differentiation of human mesenchymal stem cells through adenosine signaling. Biomacromolecules, 16(3), 1050–1061. doi:10.1021/acs.biomac.5b00099 [PubMed: 25686297]

Katagiri T, Yamaguchi A, Ikeda T, Yoshiki S, Wozney JM, Rosen V, … Suda T (1990). The non-osteogenic mouse pluripotent cell line, C3H10T1/2, is induced to differentiate into osteoblastic cells by recombinant human bone morphogenetic protein-2. Biochem Biophys Res Commun, 172(1), 295–299. [PubMed: 1699539]

Komori T, Yagi H, Nomura S, Yamaguchi A, Sasaki K, Deguchi K, … Kishimoto T (1997). Targeted disruption of Cbfa1 results in a complete lack of bone formation owing to maturational arrest of osteoblasts. Cell, 89(5), 755–764. [PubMed: 9182763]

Laurencin CT, Ashe KM, Henry N, Kan HM, & Lo KWH (2014). Delivery of small molecules for bone regenerative engineering: preclinical studies and potential clinical applications. Drug Discovery Today, 19(6), 794–800. doi:10.1016/j.drudis.2014.01.012 [PubMed: 24508820]

Liu X, & Ma PX (2009). Phase separation, pore structure, and properties of nanofibrous gelatin scaffolds. Biomaterials, 30(25), 4094–4103. doi:10.1016/j.biomaterials.2009.04.024 [PubMed: 19481080]

Liu Y, Hunziker EB, Randall NX, de Groot K, & Layrolle P (2003). Proteins incorporated into biomimetically prepared calcium phosphate coatings modulate their mechanical strength and dissolution rate. Biomaterials, 24(1), 65–70. doi:10.1016/S0142-9612(02)00252-1 [PubMed: 12417179]

Liu Y, Yao Q, & Sun H (2018). Prostaglandin E2 Modulates Bone Morphogenetic Protein-2 Induced Osteogenic Differentiation on a Biomimetic 3D Nanofibrous Scaffold. Journal of Biomedical Nanotechnology, 14(4), 747–755. doi:10.1166/jbn.2018.2490 [PubMed: 31352948]

Lo KWH, Ashe KM, Kan HM, & Laurencin CT (2012). The role of small molecules in musculoskeletal regeneration. Regenerative medicine, 7(4), 535–549. doi:10.2217/rme.12.33 [PubMed: 22817627]

Loi F, Córdova LA, Pajarinen J, Lin TH, Yao Z, & Goodman SB (2016). Inflammation, fracture and bone repair. Bone, 86, 119–130. doi:10.1016/j.bone.2016.02.020 [PubMed: 26946132]

McBeath R, Pirone DM, Nelson CM, Bhadriraju K, & Chen CS (2004). Cell shape, cytoskeletal tension, and RhoA regulate stem cell lineage commitment. Dev Cell, 6(4), 483–495. [PubMed: 15068789]

Miszuk JM, Xu T, Yao Q, Fang F, Childs JD, Hong Z, … Sun H (2018). Functionalization of PCL-3D electrospun nanofibrous scaffolds for improved BMP2-induced bone formation. Applied Materials Today, 10, 194–202. doi:10.1016/j.apmt.2017.12.004 [PubMed: 29577064]

Oyane A, Kim HM, Furuya T, Kokubo T, Miyazaki T, & Nakamura T (2003). Preparation and assessment of revised simulated body fluids. J Biomed Mater Res A, 65(2), 188–195. doi:10.1002/jbm.a.10482 [PubMed: 12734811]

Park KW, Waki H, Choi S-P, Park K-M, & Tontonoz P (2010). The small molecule phenamil is a modulator of adipocyte differentiation and PPARgamma expression. Journal of lipid research, 51(9), 2775–2784. doi:10.1194/jlr.M008490 [PubMed: 20519739]

Qadir M, Jakir Hossan M, Gafur M, & Mainul Karim M (2014). Preparation and Characterization of Gelatin-Hydroxyapatite Composite for Bone Tissue Engineering (Vol. 14).

S M Arsad M, M Lee P, & Kong Hung L (2011). Synthesis and Characterization of Hydroxyapatite Nanoparticles and β-TCP Particles (Vol. 7).

Shih Y-RV, Hwang Y, Phadke A, Kang H, Hwang NS, Caro EJ, … Varghese S (2014). Calcium phosphate-bearing matrices induce osteogenic differentiation of stem cells through adenosine signaling. Proc Natl Acad Sci U S A, 111(3), 990–995. doi:10.1073/pnas.1321717111 [PubMed: 24395775]

Tontonoz P, Hu E, & Spiegelman BM (1994). Stimulation of adipogenesis in fibroblasts by PPAR gamma 2, a lipid-activated transcription factor. Cell, 79(7), 1147–1156. [PubMed: 8001151]

Lo WH, K., Ulery D, B., Deng M, Ashe M, K., & Laurencin T, C. (2011). Current Patents on Osteoinductive Molecules for Bone Tissue Engineering. Recent Patents on Biomedical Engineering, 4(3), 153–167. Retrieved from https://www.ingentaconnect.com/content/ben/biomeng/2011/00000004/00000003/art00002

Wen L, Wang Y, Wang H, Kong L, Zhang L, Chen X, & Ding Y (2012). L-type calcium channels play a crucial role in the proliferation and osteogenic differentiation of bone marrow mesenchymal stem cells. Biochem Biophys Res Commun, 424(3), 439–445. doi:10.1016/j.bbrc.2012.06.128 [PubMed: 22771798]

Xu T, Miszuk JM, Zhao Y, Sun H, & Fong H (2015). Electrospun polycaprolactone 3D nanofibrous scaffold with interconnected and hierarchically structured pores for bone tissue engineering. Adv Healthc Mater, 4(15), 2238–2246. doi:10.1002/adhm.201500345 [PubMed: 26332611]

Yamaguchi A, Sakamoto K, Minamizato T, Katsube K, & Nakanishi S (2008). Regulation of osteoblast differentiation mediated by BMP, Notch, and CCN3/NOV. Japanese Dental Science Review, 44(1), 48–56. doi:10.1016/j.jdsr.2007.11.003

Yang X, Li Y, Liu X, Zhang R, & Feng Q (2018). In Vitro Uptake of Hydroxyapatite Nanoparticles and Their Effect on Osteogenic Differentiation of Human Mesenchymal Stem Cells. Stem cells international, 2018, 2036176–2036176. doi:10.1155/2018/2036176 [PubMed: 30018644]

Yao Q, Liu Y, Selvaratnam B, Koodali RT, & Sun H (2018). Mesoporous silicate nanoparticles/3D nanofibrous scaffold-mediated dual-drug delivery for bone tissue engineering. J Control Release, 279, 69–78. doi:10.1016/j.jconrel.2018.04.011 [PubMed: 29649529]

Yao Q, Liu Y, & Sun H (2018). Heparin-dopamine functionalized graphene foam for sustained release of bone morphogenetic protein-2. J Tissue Eng Regen Med, 12(6), 1519–1529. doi:10.1002/term.2681 [PubMed: 29702734]

Yao Q, Liu Y, Tao J, Baumgarten KM, & Sun H (2016). Hypoxia-Mimicking Nanofibrous Scaffolds Promote Endogenous Bone Regeneration. ACS Appl Mater Interfaces, 8(47), 32450–32459. doi:10.1021/acsami.6b10538 [PubMed: 27809470]

Yao Q, Sandhurst ES, Liu Y, & Sun H (2017). BBP-Functionalized Biomimetic Nanofibrous Scaffold Can Capture BMP2 and Promote Osteogenic Differentiation. Journal of materials chemistry. B, 5(26), 5196–5205. doi:10.1039/C7TB00744B [PubMed: 29250330]

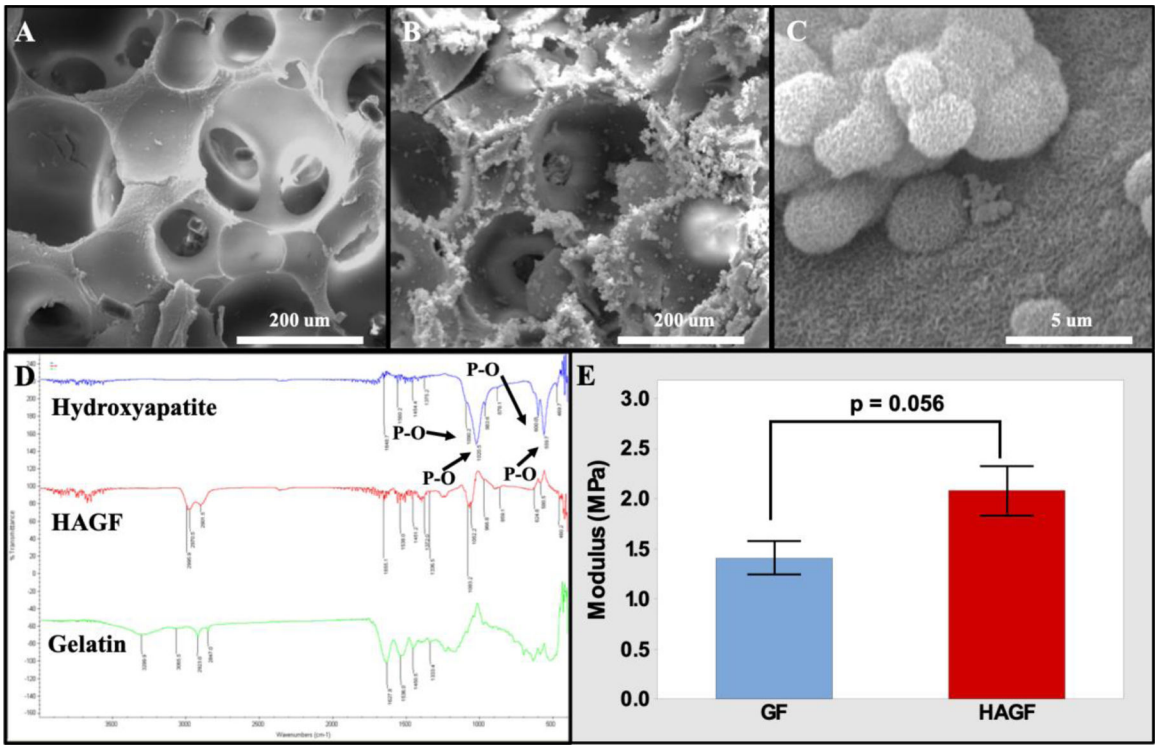

Figure 1.

Scanning electron microscopy Images of scaffolds. GF (A) and HAGF scaffold (B) at 500X and HAGF scaffold at 20000X (C) magnifications respectively. (D) FTIR peaks of gelatin type B (green), hydroxyapatite (blue), and HAGF scaffold (red). (E) HAGF scaffold showed stronger compression strength. HAGF: hydroxyapatite-coated nanofibrous gelatin.

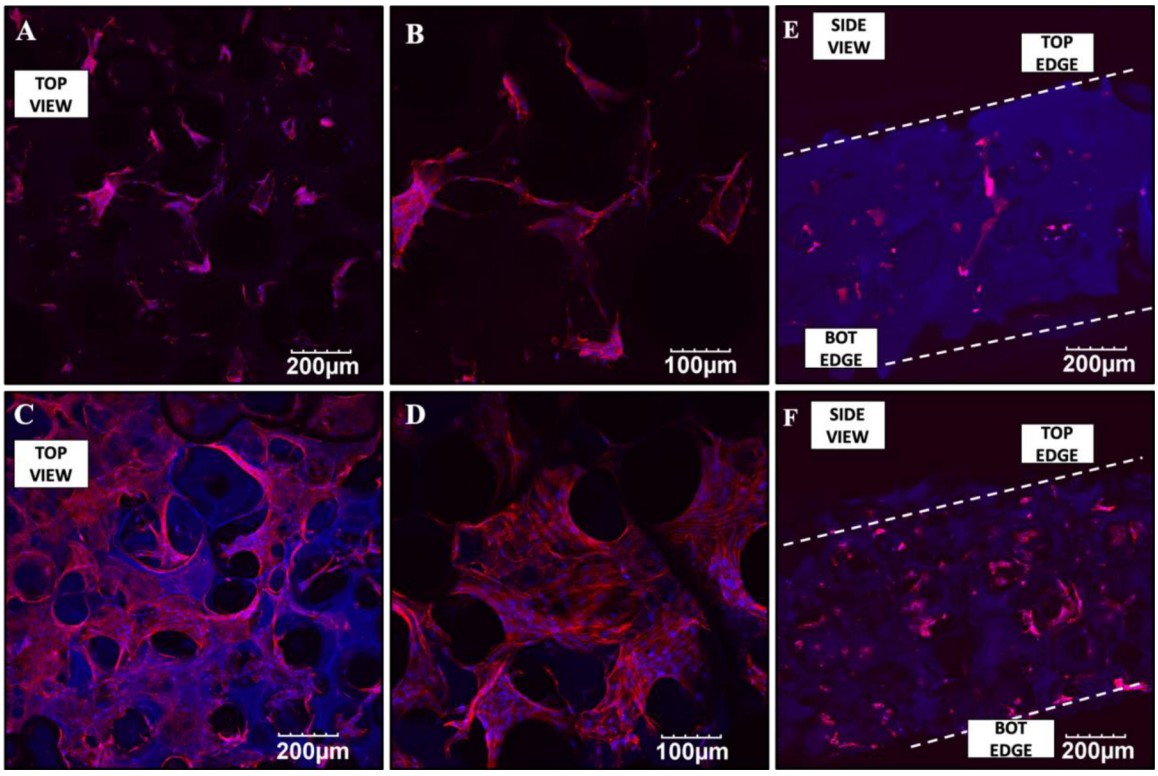

Figure 2.

Confocal images of MC3T3-E1 in gelatin nanofibrous (GF) scaffolds at magnifications 10X (**A**) and 20X (**B**) and in hydroxyapatite-coated gelatin nanofibrous (HAGF) scaffolds with magnifications at 10X (**C**) and 20X **(D**) after 5 days. Cross-section views of confocal displays cell attachment in both scaffold types (**E,F**).

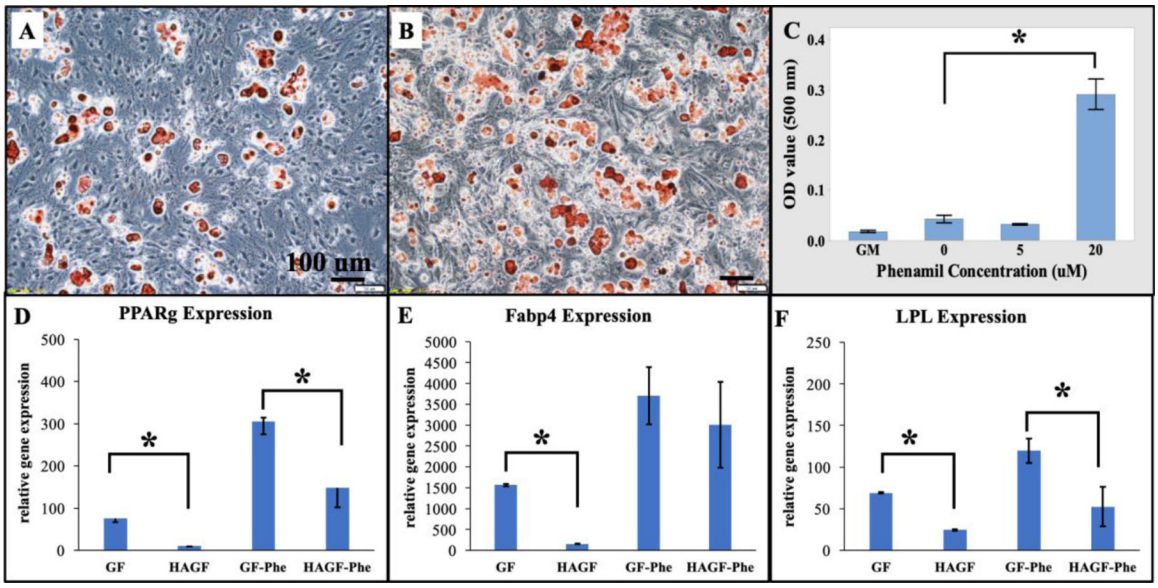

Figure 3.

Phenamil and HAGF scaffold regulates adipogenesis in C3H10T1/2 cells. (A-B) Oil Red O staining (10X) showed increasing lipid content in adipogenic medium on 2D wells at 0 micromolar (uM) (**A**) and 20 uM (**B**). Lipid content sequentially increased as phenamil concentration increased (C) on 2D plate. In 3D HAGF scaffold, adipogenic gene expressions of (D) peroxisome proliferator-activated receptor gamma (PPARg), (E) fatty acid-binding protein (Fabp4), and (F) lipoprotein lipase (LPL) reduced after 14d cell culture in adipogenic medium under phenamil treatment at 20 uM (n=3). uM = μM.*$p<0.05$. HAGF: hydroxyapatite-coated nanofibrous gelatin scaffold. GF: nanofibrous gelatin scaffold. GF-Phe: nanofibrous gelatin scaffold with phenamil treatment. HAGF-Phe: hydroxyapatite-coated nanofibrous gelatin scaffold with phenamil treatment.

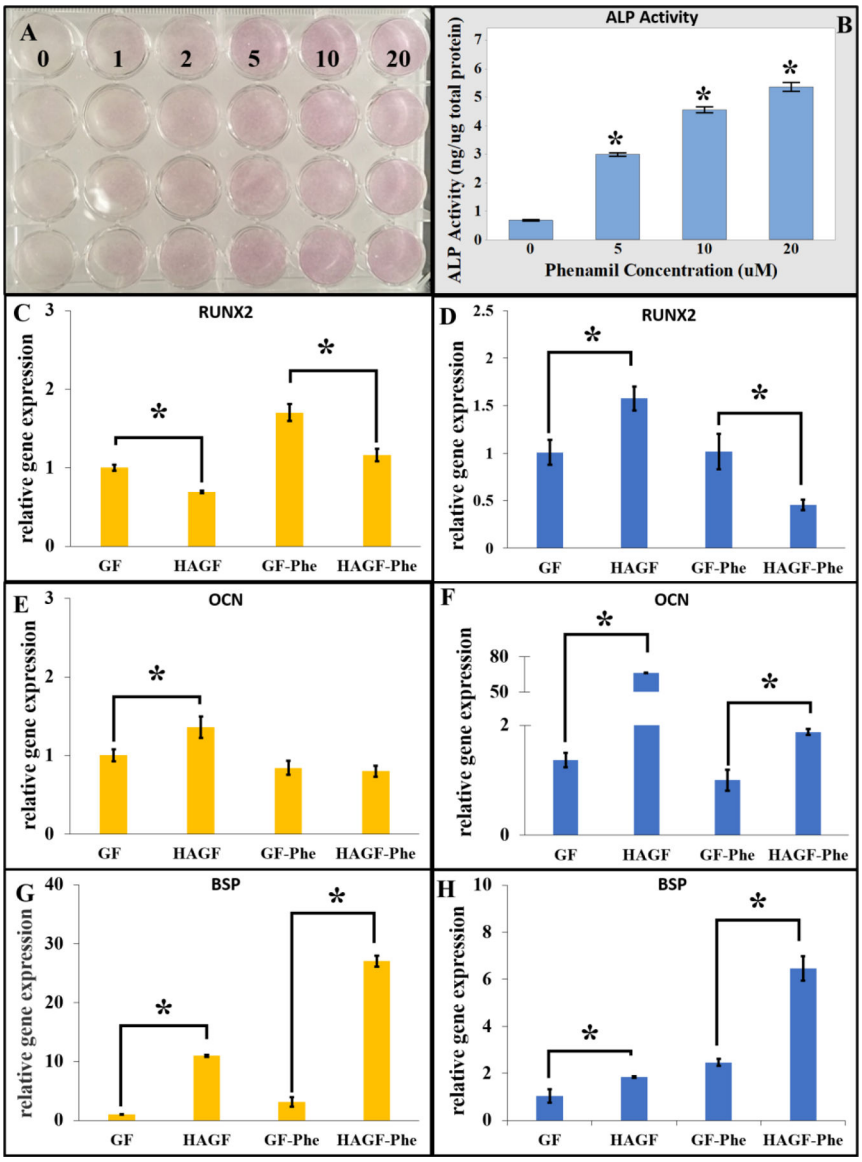

Figure 4.

Phenamil modulates MC3T3-E1 osteoblastic differentiation. (**A**) Alkaline phosphatase (ALP) staining showed increased activity in MC3T3-E1 cells with phenamil addition (purple color) at concentrations of 0 to 20 micromolar (uM). (**B**) Quantitative ALP activity exhibited by phenamil concentration-dependency over 7 d culture (n=3). Gene expression of MC3T3-E1 cells on different scaffold were observed on day 7 (**yellow**) and day 14 (**blue**). Hydroxyapatite and phenamil affected genome expression for (**C,D**) RUNX2, (**E,F**) OCN and (**G,H**) BSP after 7 d or 14 d (n=3). *p<0.05. RUNX2: Runt-related transcription factor. OCN: osteocalcin. BSP: bone sialoprotein.

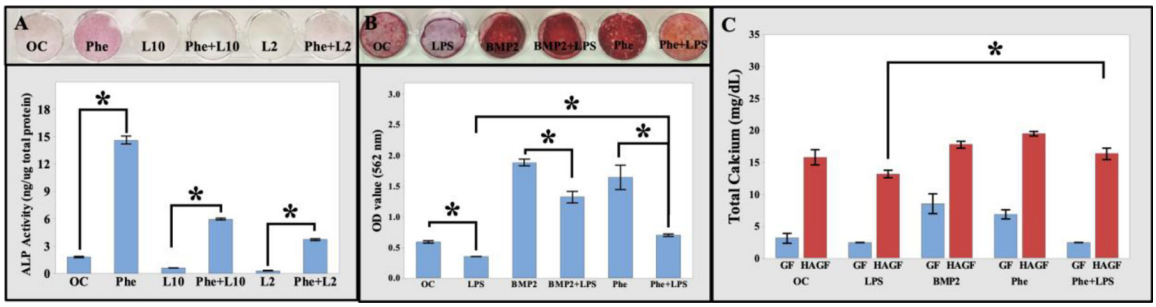

Figure 5.

Phenamil rescued LPS-inhibited osteogenic activity. (**A**) ALP staining and quantitative data of MC3T3-E1 cells showed phenamil-rescued LPS-induced ALP (purple color). (**B**) Alizarin Red S (10X) staining showed increasing calcium content when treated with BMP2 or phenamil for 28 d. No calcium content detected in LPS. Quantitative results of calcium content when treated with BMP2 and phenamil for 28 d (n=3). (**C**) HAGF scaffold increased MC3T3-E1 calcium mineralization before and after stimulation with BMP2 and phenamil after 28 d cell culture in osteogenic medium (n=3). BMP2 (200 ng/mL). Phenamil (Phe, 20 mM). L10 (10 ng/mL LPS). L2 (2 mg/mL LPS). *p<0.05. LPS: lipopolysaccharide. BMP2: bone morphogenetic protein 2.

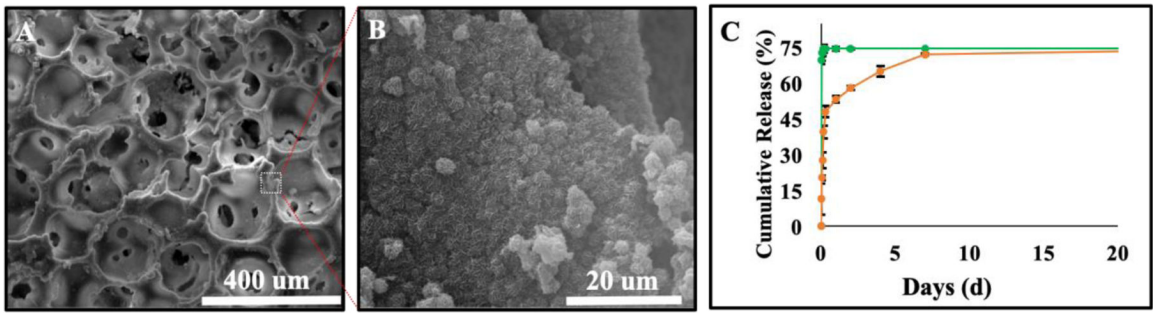

Figure 6.

Phenamil release kinetic from HAGF scaffold. SEM imaging of two-step HA deposition used to encapsulate phenamil onto HAGF scaffold at 300X (A) and 5000X (B) magnification. (C) Phenamil was either absorbed (green) or encapsulated (orange) onto HAGF scaffold for release curve determination (n=3).